

# Solid-state NMR proves the presence of penta-coordinated Sc site in MIL-100(Sc)

R. Giovine,<sup>[a]</sup> C. Volkringer,<sup>[a],[b]</sup> S. E. Ashbrook,<sup>[c]</sup> J. Trébosc,<sup>[a]</sup> D. McKay,<sup>[c]</sup> T. Loiseau,<sup>[a]</sup> J.-P. Amoureux,<sup>[a],[d]</sup> O. Lafon,<sup>[a],[b]</sup> F. Pourpoint,<sup>\*[a]</sup>

**Abstract:** Advanced solid-state NMR methods and first-principles calculations demonstrate for the first time the formation of penta-coordinated scandium sites. These coordinatively unsaturated sites were shown during the thermal activation of scandium-based Metal-Organic Frameworks (MOFs). <sup>45</sup>Sc NMR experiment allows their specific observation in activated Sc<sub>3</sub>BTB<sub>2</sub> and MIL-100(Sc) MOFs. The assignment of the ScO<sub>5</sub> groups is supported by the DFT calculations of NMR parameters. The presence of ScO<sub>5</sub> Lewis acid sites in MIL-100(Sc) explains furthermore its catalytic activity. We also introduce the first NMR experiment to probe <sup>13</sup>C-<sup>45</sup>Sc distances. This advanced solid state NMR pulse sequence allows us to demonstrate the shrinkage of the MIL-100(Sc) network when the activation temperature raises.

## Introduction

Metal-Organic Frameworks (MOFs) materials offer rich physical and chemical properties due to their adjustable architectures and porosity.<sup>[1]</sup> Thus, they present possible applications in multiple domains including gas storage, heterogeneous catalysis, drug delivery... Amongst the wide variety of MOFs, MIL-100 compound exhibits a porous framework incorporating large cavities with diameter up to 34 Å, related to the MTN zeolite topology (ZSM-39). Firstly reported with chromium(III),<sup>[2]</sup> MIL-100 has then been isolated with other trivalent metals, such as iron,<sup>[3]</sup> aluminium,<sup>[4]</sup> vanadium,<sup>[5]</sup> scandium<sup>[6, 7]</sup> or indium.<sup>[8]</sup> These MOFs have been widely investigated owing to their numerous interesting properties including (i) high surface areas, (ii) Lewis-acidity, and (iii) remarkable thermal stability.<sup>[4, 9]</sup> In particular, the Lewis acidity of activated MIL-100(Al or Cr) has been ascribed to the presence of penta-coordinated metal sites (AlO<sub>5</sub> or CrO<sub>5</sub>),<sup>[9-11]</sup> which are generated upon thermal activation. The CrO<sub>5</sub> sites were detected by CO sorption Infra-Red (IR) study,<sup>[9, 11]</sup> whereas

the AlO<sub>5</sub> ones were observed either by solid-state Nuclear Magnetic Resonance (NMR)<sup>[12]</sup> or IR<sup>[13]</sup> spectroscopy. Conversely, to the best of our knowledge, the nature of Lewis acid sites in MIL-100(Sc) has remained elusive.<sup>[14, 15]</sup> IR and H<sub>2</sub> adsorption studies have recently demonstrated the formation of five-fold coordinated scandium atoms, ScO<sub>5</sub>, upon the thermal activation of another MOF: [Sc<sub>3</sub>O(BTB)<sub>2</sub>(H<sub>2</sub>O)<sub>3</sub>](OH)(H<sub>2</sub>O)<sub>5</sub>(DMF), with H<sub>3</sub>BTB = 1,3,5-tris(4-carboxyphenyl) benzene, called Sc<sub>3</sub>BTB<sub>2</sub> hereafter.<sup>[16]</sup> Nevertheless, the Lewis acidity of this MOF has not been investigated and hence it has not been possible to relate the Lewis acidity of Sc-based MOFs to the formation of ScO<sub>5</sub> sites.

<sup>45</sup>Sc solid-state NMR a priori looks to be a promising technique to study the local environment of Sc atoms. <sup>45</sup>Sc nucleus has favorable NMR properties, including 100% natural abundance and a gyromagnetic ratio close to that of <sup>13</sup>C,  $\gamma(^{45}\text{Sc}) \approx 0.967\gamma(^{13}\text{C})$ .<sup>[6, 17, 18]</sup> Furthermore, <sup>45</sup>Sc chemical shifts are known to be very sensitive to the coordination number of the scandium<sup>[17, 19, 20]</sup> and their assignment can be supported by Density Functional Theory (DFT) calculations,<sup>[19, 21, 22]</sup> notably in Sc-based MOFs.<sup>[15]</sup> For Sc nuclei surrounded by similar atoms, it has been shown that the <sup>45</sup>Sc isotropic chemical shift decreases when the coordination number of the scandium site increases.<sup>[17, 22]</sup> Nevertheless, the <sup>45</sup>Sc isotropic chemical shift is also quite sensitive to the other structural differences, such as bond angles and bond distances<sup>[19, 20]</sup> and hence the shift regions of the different Sc coordinations in different families of materials overlap heavily. Furthermore, this spin-7/2 isotope is subject to large quadrupolar interactions<sup>[19, 20]</sup> and hence the second-order quadrupolar broadening can obscure the chemical shift information. Such quadrupolar interaction is especially large for asymmetrical Sc environments, such as ScO<sub>5</sub>. An additional difficulty for the NMR detection of <sup>45</sup>ScO<sub>5</sub> sites is the low concentration of those sites, since most materials contain mainly six, seven or eight-coordinated scandium environments.<sup>[17, 20]</sup> Despite these difficulties, penta-coordinated Sc sites have been recently observed by solid-state NMR in Sc-doped BaZrO<sub>3</sub> containing oxygen vacancies.<sup>[16]</sup> However, in MOFs, only hexa-coordinated Sc sites have been seen by solid-state NMR so far.<sup>[6, 15]</sup>

The NMR observation of carbon-scandium proximities would also provide valuable information about the structure of Sc-based MOFs. However, an instrumental limitation of NMR spectroscopy is that usual multiple channels NMR probes cannot be tuned simultaneously to two close Larmor frequencies, such as those of <sup>13</sup>C and <sup>45</sup>Sc isotopes (100.6 and 97.2 MHz, respectively at the magnetic field of 9.4 T). Therefore, to the best of our knowledge, <sup>13</sup>C-<sup>45</sup>Sc double resonance experiments have not been reported so far. Nevertheless, we have demonstrated

[a] R.G., Prof C.V., Dr J.T., Dr T.L., Prof J.-P.A., Prof O.L., Dr F.P. Univ. Lille, CNRS, ENSCL, Centrale Lille, Univ. Artois, UMR 8181 - UCCS -Unité de Catalyse et Chimie du Solide, F-59000 Lille, France frederique.pourpoint@ensc-lille.fr

[b] Prof C.V, Prof O.L., Institut Universitaire de France, 1 rue Descartes, 75231 Paris Cedex 5, France

[c] Prof S.E.A., Dr D. MK EaStCHEM and School of Chemistry, University of St. Andrews, Purdie Building, North Haugh, St. Andrews, Fife, KY16 9ST, Scotland

[d] Prof J.-P.A. Bruker, Biospin, Wissembourg, France

Supporting information for this article is given via a link at the end of the document.

recently that the use of a frequency splitter<sup>[23]</sup> can circumvent this limitation since this device allows tuning and matching a single probe channel to two close frequencies. We have notably used such device to acquire double-resonance  $^{27}\text{Al}$ - $^{13}\text{C}$ <sup>[24, 25]</sup> and  $^{13}\text{C}$ - $^{51}\text{V}$ <sup>[26]</sup> solid-state NMR experiments.

Herein, we demonstrate the formation of  $\text{ScO}_5$  sites during the thermal activation of  $\text{Sc}_3\text{BTB}_2$  using  $^1\text{H}$  and  $^{45}\text{Sc}$  NMR at high magnetic field. The assignment of penta-coordinated Sc site is supported by DFT calculations. Furthermore, during the thermal activation of MIL-100(Sc), we also observe  $^{45}\text{Sc}$  NMR signals at similar chemical shifts, which demonstrate the presence of penta-coordinated scandium species, which can react as Lewis acid sites. We report furthermore the first NMR observation of  $^{13}\text{C}$ - $^{45}\text{Sc}$  proximities in activated MIL-100(Sc). These double-resonance  $^{13}\text{C}$ - $^{45}\text{Sc}$  experiments allow observing the shrinkage of MOFs structure upon its thermal activation.

## Results and Discussion

### 1. Structure and X-Ray diffraction of $\text{Sc}_3\text{BTB}_2$ and MIL-100(Sc)

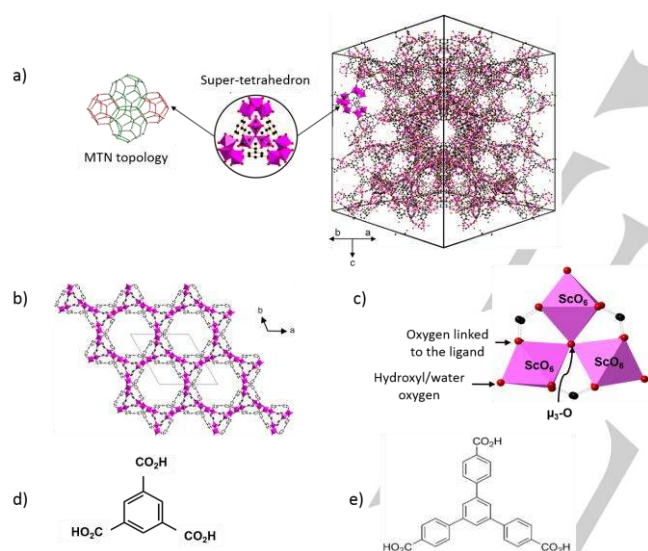


**Figure 1.** Representation of (a) the MTN topology of MIL-100(Sc), (b) the structure of  $\text{Sc}_3\text{BTB}_2$  (c) the trigonal trimer of scandium; (d) the trimesate ligand found in the MIL-100(Sc) structure; and (e) the 1,3,5-tris(4-carboxyphenyl)benzene ligand found in the  $\text{Sc}_3\text{BTB}_2$  structure.

The structures of  $\text{Sc}_3\text{BTB}_2$  and MIL-100(M) (M= metal) have been solved by X-ray diffraction (XRD) of single-crystals.<sup>[2, 27]</sup> The building unit of  $\text{Sc}_3\text{BTB}_2$  and MIL-100(Sc) consists in a trimer of corner sharing  $\text{ScO}_6$  octahedra linked by a  $\mu_3\text{-oxo}$  ligand. Thus, each  $\text{Sc}^{3+}$  ion is hexa-coordinated to: (i) one  $\mu_3\text{-O}$ , (ii) four oxygen atoms from carboxylate groups, and (iii) a terminal hydroxyl group or a terminal water molecule (Fig. 1c). Carboxylate ligands bridge the corner sharing  $\text{ScO}_6$  octahedra of

the trimer. Conversely, the ligands differ between  $\text{Sc}_3\text{BTB}_2$  and MIL-100(Sc). The former is built up from 1,3,5-tris(4-carboxyphenyl)benzene (Fig. 1e) and the latter from trimesic acid (Fig. 1d). The crystal structures of  $\text{Sc}_3\text{BTB}_2$  and MIL-100(Sc) also differ. The  $\text{Sc}_3\text{BTB}_2$  crystallizes in the hexagonal space group  $P\bar{6}2c$  forming hexagonal channels with a diameter of approximately 23 Å (Fig. 1b). Its unit cell contains two crystallographically inequivalent scandium sites. Conversely, MIL-100(Sc) adopts the topology corresponding to the MTN zeolite (Fig. 1a) and its unit cell includes seven crystallographically inequivalent scandium sites.<sup>[16]</sup>

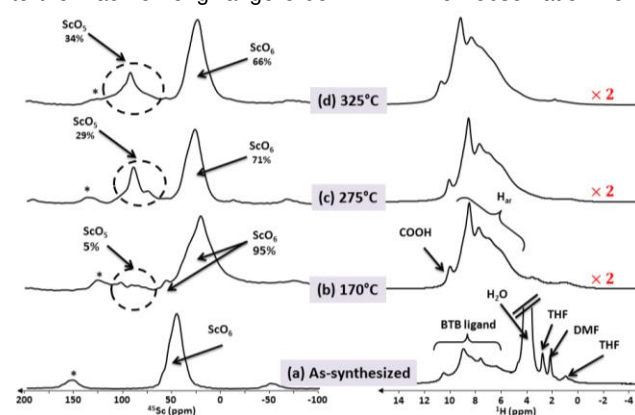
X-ray thermogravimetric analysis allows probing modifications of the long-range positional order versus temperature for  $\text{Sc}_3\text{BTB}_2$  and MIL-100(Sc) (Fig. S4 and S5, respectively). Up to 400°C, no drastic change occurs in the diffractogram of  $\text{Sc}_3\text{BTB}_2$  indicating that the crystal structure of this MOF is preserved up to this temperature. Above 400°C, the diffraction peaks vanish because of the ligand decomposition, which results in a collapse of the crystal structure. The rehydration of the different compounds activated at different temperatures does not perturb the 3D organization of the structure, since their corresponding powder X-ray diffraction patterns are similar (Fig. S6).

For MIL-100(Sc), no significant change occurs in terms of diffractogram upon heating up to 220°C (blue curves in Fig. S5). Above 220°C, diffraction Bragg peaks progressively broaden and decrease in intensity suggesting the formation of defects (green curves). At 300°C, diffraction peaks vanish, which indicates the collapse of the MIL-100(Sc) framework (red curves).

### 2. Solid-state NMR spectra of $\text{Sc}_3\text{BTB}_2$

#### 2.1. 1D NMR spectra

As already shown for MIL-100(Al or Cr), the penta-coordinated metal sites cannot be observed by diffraction techniques owing to their lack of long-range order.<sup>[9-11, 27]</sup> Their observation hence



requires techniques, such as IR and NMR, which can probe the local structure at atomic level.<sup>[9, 11-13]</sup> Fig. 2 displays the  $^{45}\text{Sc}$  and  $^1\text{H}$  NMR spectra of  $\text{Sc}_3\text{BTB}_2$  as-synthesized materials (Fig. 2a) and after thermal treatment up to 325°C (Fig. 2b-d) recorded at high magnetic field (18.8T).

**Figure 2.**  $^{45}\text{Sc}$  (left) and  $^1\text{H}$  (right) NMR spectra of  $\text{Sc}_3\text{BTB}_2$ : (a) as-synthesized; (b-d) after thermal treatment under vacuum of one night at (b) 170, (c) 275 and (d) 325 °C. The spectra were recorded at 18.8 T and a MAS frequency of  $\nu_{\text{R}} = 20$  kHz. Spinning side bands are labeled with \*. The vertical scale of the (b-d)  $^1\text{H}$  spectra is multiplied by 2 compared to that in (a).

$^{45}\text{Sc}$  NMR spectrum of the as-synthesized material shows a single resonance around 50 ppm, assigned to a scandium species in an octahedral environment ( $\text{ScO}_6$ ). This assignment is in agreement with the literature.<sup>[6, 15]</sup> The resolution does not allow distinguishing the two scandium crystallographic sites, even if the line-shape differs from the typical powder pattern of a single  $^{45}\text{Sc}$  site and must be produced by overlapping signals from distinct Sc local environments. This line subsumes the contributions of scandium sites attached to terminal hydroxo and aqua ligands in the trinuclear  $\mu_3$ -oxo-centered inorganic sub-unit. When the temperature increases at 170 °C (Fig. 2b), a high field shift of the most intense  $^{45}\text{Sc}$  signal is observed. This shift is tentatively ascribed to the evacuation of the pores and the flips of the ligand phenyl rings around the single bonds between  $\text{sp}^2$  hybridized carbon atoms (Fig. 1e). For the terephthalic ligand, such phenyl flips have been observed using  $^2\text{H}$  NMR.<sup>[28]</sup> Moreover, the lineshape of  $\text{ScO}_6$  signal at 170 °C is broader than for the as-synthesized material. Such broadening stems from a distribution in the orientation of the phenyl ring at higher temperature. Weak and deshielded  $^{45}\text{Sc}$  peaks are also observed at 170 °C. Their intensities grow when the temperature raises (compare Figs. 2c-d) to reach 34% of the total integrated intensity at 325 °C. It has been shown that the isotropic chemical shift of  $^{45}\text{Sc}$  nuclei increases for lower coordination number,<sup>[20, 22]</sup> and especially the  $^{45}\text{Sc}$  signals of  $\text{ScO}_5$  sites are more deshielded than those of  $\text{ScO}_6$  ones.<sup>[29]</sup> Therefore these sites can be assigned to penta-coordinated scandium. This attribution is in agreement with the literature where the  $\text{ScO}_5$  sites have been evidenced by IR and  $\text{H}_2$  adsorption in activated  $\text{Sc}_3\text{BTB}_2$ .<sup>[16]</sup> But to the best of our knowledge, the NMR observation of  $\text{ScO}_5$  site in MOFs has not been reported so far. Furthermore, the fraction of 34% of penta-coordinated scandium is in agreement with the structure (Fig. 3) and with results already published for analogous MOFs.<sup>[3, 9, 10]</sup> As stated above, the slight disorder and the emergence of the penta-coordinated sites observed by NMR do not lead to main changes in the long-range order of the structure according to the XRD (Fig. S4).

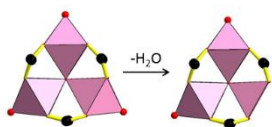


**Figure 3.** Illustration of the dehydration process in scandium trimer  $\text{Sc}_3(\mu_3\text{-oxo})$  and the formation of the penta-coordinated Sc site.

$^1\text{H}$  NMR spectrum of the as-synthesized material is dominated by a high intensity water signal resonating at 3.7 ppm (Fig. 2a). To better display, its intensity has been cut. Two other groups of signals are observed in the spectrum. Between 0 and 3 ppm, low intensity signals are assigned to residual solvent or

impurities trapped into the pores, while between 5 and 12 ppm, signals are assigned to the ligand. The more precise assignment of those resonances requires 2D correlation spectra and is beyond the scope of this article. When the temperature increases to 170 °C (Fig. 2b), the water signal dramatically decreases and the intensities of the peaks resonating between 0 and 3 ppm strongly decrease. This observation is consistent with volatiles species trapped into the pores (solvent), which are evacuated at high temperature. At 170 °C, a broad peak is observed at 3.8 ppm and is ascribed to  $\text{H}_2\text{O}$  and OH attached to Sc atoms. The intensity of this peak decreases at 275 and 325 °C, which is consistent with the elimination of aqua ligand (see Fig. 3). Conversely the signals resonating between 5 and 12 ppm are barely affected by the thermal activation, which suggests that the integrity of the ligand is preserved up to 325 °C. This NMR observation confirms the XRD data of Fig. S4.

## 2.2. 2D MQ-MAS spectra

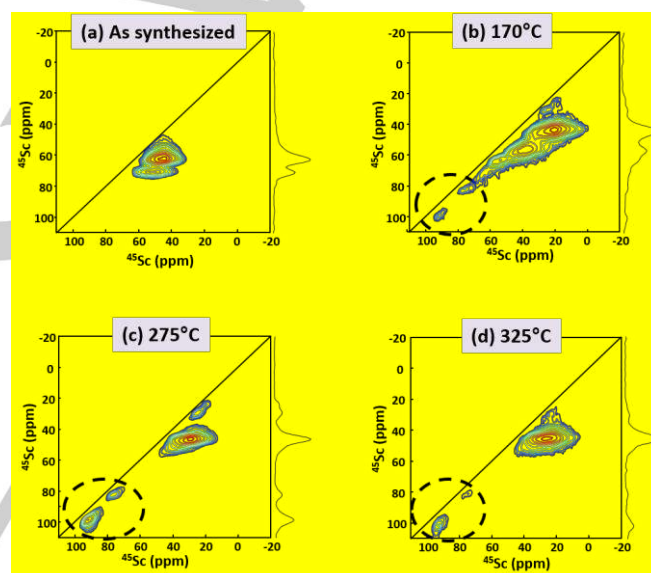


**Figure 4.**  $^{45}\text{Sc}$  3Q-MAS sheared 2D spectra of (a) as-synthesized  $\text{Sc}_3\text{BTB}_2$ , and (b-d) after thermal treatment at: (b) 170, (c) 275, and (d) 325 °C. Spectra were recorded at 18.8 T and  $\nu_{\text{R}} = 20$  kHz. The peaks inside the black circles correspond to  $\text{ScO}_5$  sites.

The resolution of  $^{45}\text{Sc}$  NMR experiments is drastically improved by acquiring 3Q-MAS 2D spectra (Fig. 4), to the extent that the two crystallographic-distinct sites of  $\text{ScO}_6$  are observable in the spectrum of the as-synthesized material (Fig. 4a). The fits of this spectrum (Fig. S9) lead to the quadrupolar parameters reported in Table S1. The relatively high  $C_Q$  values (11.7 and 13.5 MHz) suggest a non-symmetrical octahedral environment for the scandium sites. At higher temperature (170 °C, Fig. 4b), a broader distribution of quadrupolar parameters and chemical shifts is observed. At least six different scandium sites can be distinguished (Fig. S10, Table S2). Amongst them the two most deshielded signals at 77 and 92 ppm, which experience a smaller quadrupole interaction with  $C_Q \approx 8.0$  MHz, can be assigned to two penta-coordinated scandium sites. By

increasing the temperature at 275°C (Fig. 4c, Fig. S11 and Table S3) and 325°C (Fig. 4d, Fig. S12 and Table S4), the intensity of those deshielded signals increases in agreement with the 1D spectra (Fig. 2b, c and d), whereas the  $C_Q$  and  $\delta_{iso}$  values remain similar. This result suggests an increase of the amount of  $ScO_5$  in the material. To summarize, in  $Sc_3BTB_2$ , hexa- and penta-coordinated scandium sites exhibit different ranges for the NMR parameters  $C_Q$  and  $\delta_{iso}$  (see Table 1). It is noted that in the 3Q-MAS 2D spectrum of the 170°C material, the peak resonating at 66 ppm cannot be safely attributed to  $ScO_5$  or  $ScO_6$  since its quadrupolar parameters and isotropic chemical shift are not characteristic of neither scandium site.

**Table 1.** Ranges of isotropic chemical shifts and  $C_Q$  values of the penta- and hexa-coordinated sites experimentally observed in  $Sc_3BTB_2$ .

Site	$ScO_5$	$ScO_6$
$\delta_{iso}$ (ppm)	70-100	20-60
$C_Q$ / MHz	$\approx 8$	9-14

### 3. Calculation of NMR parameters of $ScO_5$ and $ScO_6$ sites

First-principles calculations of  $^{45}Sc$  NMR parameters in Sc-based MOFs were carried out to further support the assignment of  $ScO_5$  signal. However, the large number of atoms in the unit cell of  $Sc_3BTB_2$  and MIL-100(Sc) precludes DFT calculations using CASTEP code to converge within reasonable amount of time. Therefore, the DFT calculations were carried out on the MIL-88(Sc) compound. The crystalline structure of this MOF (Fig. S18a) is built from the same Sc trimers as  $Sc_3BTB_2$  and MIL-100(Sc) but with the 2,5-dihydroxyterephthalate ligand (Fig. S18b). However, its structure can be described by a much smaller unit cell. We performed first the calculations on the unmodified MIL-88(Sc) structure (see Table S5).<sup>[30]</sup> The difference in  $\delta_{iso}$  between  $ScO_6$  sites, (a,d) on the one hand and (b,c,e,f) on the other hand, is about 6-7 ppm, which is similar to that between the two  $ScO_6$  sites of  $Sc_3BTB_2$  (see Table S1). The calculated  $C_Q$  values of  $ScO_6$  site in MIL-88(Sc) are comparable to those measured for similar Sc environments in  $Sc_3BTB_2$  (see Table S1). Calculations were also performed on the modified MIL-88(Sc) structure in which a  $H_2O$  ligand had been removed from the structure in order to form a five-fold coordinated scandium (see Table S6). For such structure, the DFT calculations predict distinct chemical shifts for the five  $ScO_6$  sites contained within the unit cell. The  $\delta_{iso}$  of (a) and (f) sites are about 8-9 ppm higher than that of (d) site and 17-19 ppm higher than that of (b) and (c) sites. Such differences are similar to the one measured for the three most shielded  $ScO_6$  sites of  $Sc_3BTB_2$  heated at 275°C (see Table S3). The calculated  $C_Q$  values of  $ScO_6$  site in modified MIL-88(Sc) agree reasonably well with those measured for those sites in  $Sc_3BTB_2$  heated at 170, 275 or 325°C (see

Table S1 to S4). Furthermore, the DFT calculations predict a  $\delta_{iso}$  for the  $ScO_5$  site, which is 74 ppm higher than that of the most shielded  $ScO_6$  site. Such prediction agrees with the measured isotropic chemical shift difference between sites (a) and (f) in  $Sc_3BTB_2$  heated at 275°C (see Table S3) as well as sites (a) and (d) in  $Sc_3BTB_2$  heated at 325°C (see Table S4). Furthermore, the higher isotropic chemical shift of  $ScO_5$  site with respect to  $ScO_6$  one is consistent with the already reported increase in isotropic chemical shift for decreasing coordination number of Sc atom.<sup>[17, 22]</sup> The calculated  $C_Q$  values of  $ScO_5$  site in modified MIL-88(Sc) is significantly higher than that measured for those sites in  $Sc_3BTB_2$  heated at 170, 275 or 325°C (see Table S1 to S4). Such discrepancy can stem from (i) the different ligands in  $Sc_3BTB_2$  and MIL-88(Sc) and (ii) the absence of NMR signals for  $^{45}Sc$  nuclei subject to large  $C_Q$  values in the 3Q-MAS 2D spectra, from which the experimental  $C_Q$  value is measured. The 3Q-MAS experiment does not excite efficiently nuclei subject to large quadrupolar interaction. Experimentally, the number of inequivalent  $^{45}Sc$  sites in  $Sc_3BTB_2$  heated at 170 and 275°C exceeds that predicted by DFT calculations for modified MIL-88(Sc). Such discrepancy stems from the structural differences between MIL-88(Sc) and  $Sc_3BTB_2$  as well as the lack of periodicity of  $ScO_5$  defects in the  $Sc_3BTB_2$  crystal contrary to the modified MIL-88(Sc) structure used for the DFT calculations.

## 4. Solid-state NMR spectra of MIL-100(Sc)

### 4.1 1D NMR spectra

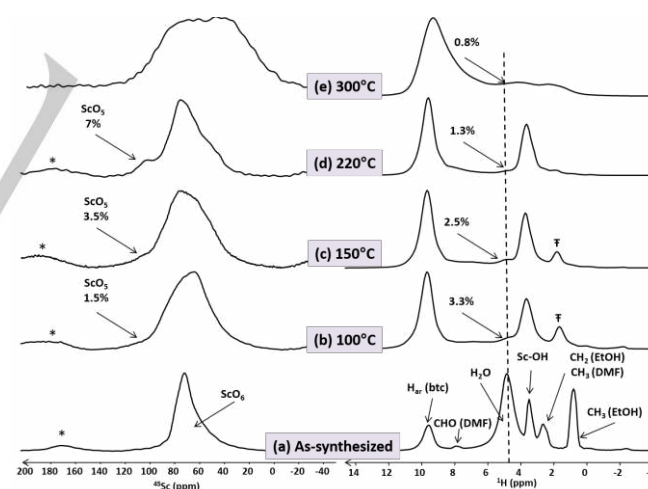


**Figure 5.**  $^{45}Sc$  (left) and  $^1H$  (right) NMR spectra of MIL-100(Sc): (a) as-synthesized and (b-d) after thermal treatment of one night at (b) 100, (c) 150, (d) 220, and (e) 300°C. The spectra were recorded at 18.8 T with a MAS frequency of  $\nu_{R} = 20$  kHz. The fraction of integrated intensity corresponding to  $^{45}ScO_5$  signal after deconvolution is indicated in (b-d) on the left. The integrated intensity of the water  $^1H$  signal after deconvolution is also indicated on the right spectra and is normalized with respect to that of water  $^1H$  signal in (a). \* and ‡ label the spinning sidebands and an impurity signal, respectively.

Fig. 5 shows the  $^{45}Sc$  and  $^1H$  NMR spectra of MIL-100(Sc) as-synthesized (Fig. 5a) and after thermal treatment at temperature ranging from 100 to 300°C (Fig. 5b-e). The  $^{45}Sc$  NMR spectrum

of the as-synthesized material is similar to that already reported and it exhibits a broad and asymmetric line-shape resonating around 70 ppm (Fig. 5a), which is assigned to  $\text{ScO}_6$  sites.<sup>[6, 15]</sup> The seven crystallographically inequivalent sites for the scandium are not resolved. As stated for the  $\text{Sc}_3\text{BTB}_2$  material, the asymmetric line-shape is attributed to the distribution of quadrupolar and chemical shift parameters. Thermal activation at temperatures ranging from 100 to 220°C produces a broadening of the  $\text{ScO}_6$  signal (Fig. 5b-e) due to a possible increase in the quadrupolar interaction. Moreover, a weak resonance at about 100 ppm becomes more intense for higher activation temperature. The deconvolution of the  $^{45}\text{Sc}$  signals is shown in Fig. S7 for MIL-100(Sc) activated at 220°C. Thus, the signal with a resonance frequency higher than  $\text{ScO}_6$  site is assigned to  $\text{ScO}_5$  environment since: (i) the results obtained in the first part of this article prove that the isotropic chemical shift of  $\text{ScO}_5$  is higher than that corresponding to  $\text{ScO}_6$  sites, (ii) in MIL-100(Al or Cr), thermal activation removes the aqua ligands of  $\text{AlO}_6$  sites and hence forms Lewis acid  $\text{AlO}_5$  or  $\text{CrO}_5$  sites, and activated MIL-100(Sc) is also a Lewis acid catalyst,<sup>[14, 15]</sup> and (iii) this signal cannot correspond to a  $^{45}\text{Sc}$  satellite transition since a corresponding peak is observed in the 3Q-MAS spectrum (see below). As seen in Fig. 5, the integrated intensity fraction corresponding to the most deshielded  $^{45}\text{Sc}$  signal increases from 100 to 220°C. This result indicates an increasing amount of  $\text{ScO}_5$  defects at higher activation temperature, up to 7 % of scandium sites. Nevertheless, the fraction indicated in Fig. 5 is much lower than that found in  $\text{Sc}_3\text{BTB}_2$  and MIL-100(Al) for penta-coordinated Sc or Al species, respectively.<sup>[10]</sup> This may be due to the less thermally stable structure of MIL-100(Sc), which collapses at 220 °C, while this temperature is required for  $\text{Sc}_3\text{BTB}_2$  and MIL-100(Al) in order to reach 30 % of  $\text{ScO}_5$  and  $\text{AlO}_5$  site, respectively. The  $^{45}\text{Sc}$  NMR spectrum of MIL-100(Sc) activated at 300°C displays a very broad line-shape, which indicates a large distribution of local Sc environments. Such distribution is consistent with the collapse of the MOF framework observed by X-ray diffraction (Fig. S5).

Fig. 5 also shows the  $^1\text{H}$  NMR spectra of MIL-100(Sc) after different thermal treatments. Multiple resonances are observed in the  $^1\text{H}$  NMR spectrum of the as-synthesized material (Fig. 5a), in agreement with the previously published  $^1\text{H}$  NMR spectrum of the analogous MIL-100(Al).<sup>[10]</sup> Upon heating, the intensity of water and solvent  $^1\text{H}$  signals strongly decreases, showing that thermal activation removes the physisorbed molecules in the pores. As seen in Fig. 5, thermal activation at 100°C results in a 30-fold decrease in the amount of water in MIL-100(Sc). Such dehydration at moderate temperature corresponds to the evacuation of physisorbed water,<sup>[10]</sup> which is pursued at higher temperatures (Fig. 5c-d). This water reduction at high temperature corresponds to the loss of aqua ligands, in agreement with the formation of  $\text{ScO}_5$  sites (see above). Moreover, the activated MIL-100(Sc) displays an additional  $^1\text{H}$  signal at 1.7 ppm (indicated with †), which is ascribed to impurities coming from the degradation of the DMF. This signal decreases for increasing activation temperature. The activated MIL-100(Sc) also displays a  $^1\text{H}$  signal at 3.5 ppm ascribed to Sc-OH sites. The OH signals in activated MIL-100(Sc) are broader than in the as-synthesized sample since in the latter the

exchange between OH protons and physisorbed molecules reduce  $^1\text{H}$ - $^1\text{H}$  dipolar coupling. The dramatic broadening of the  $^1\text{H}$  signals after thermal activation at 300°C (Fig. 5e) confirms the collapse of the MIL-100(Sc) structure.

#### 4.2 2D 3Q-MAS NMR spectra

Proof of the presence of  $\text{ScO}_5$  sites can be confirmed by the high resolution  $^{45}\text{Sc}$  3Q-MAS 2D spectra (Fig. 6). The one of the as-synthesized MIL-100(Sc) (Fig. 6a) displays a broad distribution of isotropic shifts due to the unresolved seven scandium sites, in contrast with  $\text{Sc}_3\text{BTB}_2$  that exhibits only two crystallographic sites (Fig. 4a). The 3Q-MAS spectrum of the MIL-100(Sc) activated at 220°C (Fig. 6b) permits to resolve the signals of  $\text{ScO}_5$  and  $\text{ScO}_6$  sites. With respect to the as-synthesized sample, the  $\text{ScO}_6$  signal (i) exhibits a narrower distribution of isotropic shifts and (ii) corresponds to a larger quadrupole interaction, since the removal of physisorbed molecules within the pores reduces the structural disorder and increases the electric field gradients for  $\text{ScO}_6$  sites. The 3Q-MAS spectrum of the MIL-100(Sc) activated at 300°C (Fig. 6c) confirms the broad distribution of  $^{45}\text{Sc}$  environments produced by the collapse of the MOF structure.

As a conclusion, the formation of  $\text{ScO}_5$  in thermally activated MIL-100(Sc) is confirmed by solid-state NMR upon temperature by removing a water molecule (Fig. 5). The presence of this coordinatively unsaturated site explains the Lewis acidity already observed in this material.<sup>[14, 15]</sup>

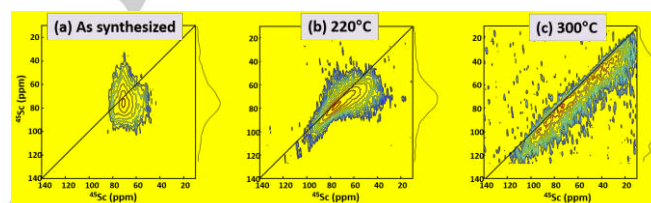


**Figure 6.**  $^{45}\text{Sc}$  3Q-MAS sheared 2D spectra at 18.8 T of (a) as-synthesized MIL-100(Sc), and after thermal treatment at (b) 220 and (c) 300°C.

#### 4.3 2D D-HMQC NMR spectra

The proximities between  $^1\text{H}$  and  $^{45}\text{Sc}$  nuclei have been probed by  $^{45}\text{Sc}\{-^1\text{H}\}$  D-HMQC 2D spectra (Fig. 7). In those spectra, the most intense correlation peak is that between the btc ligand and the  $\text{ScO}_6$  sites. A cross-peak between the signals of Sc-OH groups and  $\text{ScO}_6$  sites is also detected. This cross-peak is weak in the as-synthesized material since the proton exchange between OH groups and physisorbed water and ethanol molecules decreases the  $^1\text{H}$ - $^{45}\text{Sc}$  dipolar couplings. In the MIL-100(Sc) heated at 220°C, the cross-peak between Sc-OH proton and  $\text{ScO}_6$  sites becomes more intense since the physisorbed molecules are removed, thus preventing the proton exchange. The collapse of the structure at 300°C is confirmed by the broadening of the cross-peaks.

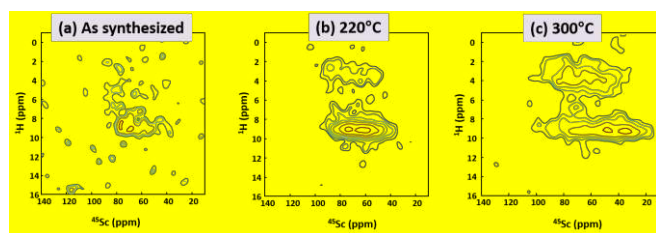


**Figure 7.**  $^{45}\text{Sc}\{-^1\text{H}\}$  D-HMQC 2D spectra of (a) as-synthesized MIL-100(Sc), and after thermal treatment at (b) 220, and (c) 300 °C. 2D spectra were recorded at 18.8 T with a spinning speed of  $\nu_{\text{R}} = 20$  kHz.

#### 4.4 $^{13}\text{C}\{-^{45}\text{Sc}\}$ S-RESPDOR NMR spectra

$^1\text{H} \rightarrow ^{13}\text{C}$  CPMAS spectra exhibit three resonances corresponding to the three distinct carbon sites of the btc ligand (Fig. S8), consistently with the previously published spectra.<sup>[6]</sup> The  $^{13}\text{C}$  signals are only marginally modified for increasing activation temperature up to 220°C. However, at 300°C a dramatic broadening occurs owing to the collapse of the MOF framework (see above). Thus, thermal activation up to 220°C leads to the formation of  $\text{ScO}_5$  sites (Fig. 5), but the integrity of the ligand is preserved below 220°C (Fig. S8).

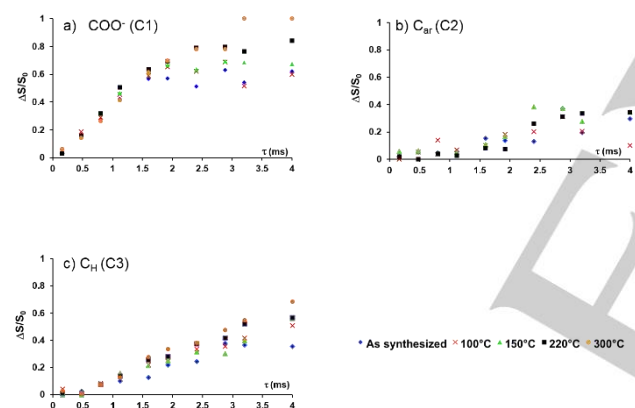


**Figure 8.** Comparison between the  $^{13}\text{C}\{-^{45}\text{Sc}\}$  SFAM-RESPDOR curves at 9.4 T and  $\nu_{\text{R}} = 12.5$  kHz for the three carbon sites: a) C3, b) C2 and c) C1 of as-synthesized MIL-100(Sc) (blue diamonds), and after thermal treatment at 100 (red crosses), 150 (green triangles), 220 (black squares) and 300°C (orange circles). The S/N of the C2 signal of the sample heated at 300°C is too low to measure the SFAM-RESPDOR fraction.

Probing  $^{13}\text{C}\{-^{45}\text{Sc}\}$  proximities is useful to detect changes in the structure of Sc-based MOFs during the heating. To this end, the  $^{13}\text{C}\{-^{45}\text{Sc}\}$  distances were measured by SFAM-RESPDOR experiments.<sup>[24]</sup> Fig. 8 displays the  $^{13}\text{C}\{-^{45}\text{Sc}\}$  S-RESPDOR signal fractions,  $\Delta\text{S}/\text{S}_0$ , as a function of the recoupling time for each of the three carbons of MIL-100(Sc) after thermal activation at different temperatures. Those heteronuclear experiments between isotopes with close Larmor frequencies were performed using a frequency splitter,<sup>[23]</sup> and a SFAM-RESPDOR sequence suitable for the splitter (see Fig. S1).<sup>[24]</sup> The comparison of the  $^{13}\text{C}\{-^{45}\text{Sc}\}$  SFAM-RESPDOR fractions for the three carbon sites shows that the dephasings of  $^{13}\text{C}$  transverse magnetization

under  $^{13}\text{C}\{-^{45}\text{Sc}\}$  dipolar couplings are the fastest for  $\text{COO}^-$  site, the slowest for  $\text{C}_{\text{ar}}$ , and intermediate for CH. These results suggest that  $d_{(\text{Sc}\dots\text{COO}^-)} < d_{(\text{Sc}\dots\text{CH})} < d_{(\text{Sc}\dots\text{C}_{\text{ar}})}$ . It is noted that a low S/N is obtained for the  $\text{C}_{\text{ar}}$  site due to the smaller efficiency of the cross polarization for the quaternary carbon (Fig. S8). Thus, the  $\Delta\text{S}/\text{S}_0$  fraction of this site exhibits a lower accuracy. For each material, the uncertainties of the signal fraction are reported in the Fig. S13-S17 using the S/N and the equation 4 of the ref.<sup>[24]</sup> Obviously for each carbon sites, the  $\Delta\text{S}/\text{S}_0$  fractions globally increase for higher activation temperature. These NMR observations indicates shorter distances between the  $^{13}\text{C}$  and  $^{45}\text{Sc}$  nuclei at higher temperature and are consistent with the shrinkage of the unit cell of MIL-100(Sc) at higher temperature. Such shrinkage has already been reported for MIL-100(Cr).<sup>[9]</sup>

## Conclusions

Solid-state NMR has demonstrated the formation of  $\text{ScO}_5$  in  $\text{Sc}_3\text{BTB}_2$  and MIL-100(Sc) upon thermal activation. To the best of our knowledge, this result represents the first NMR observation of these sites in Sc-based MOFs. In agreement with the already reported decrease in the  $^{45}\text{Sc}$  isotropic chemical shift for higher coordination number, the  $\text{ScO}_5$  signal is more deshielded than the  $\text{ScO}_6$  one. The assignment of  $\text{ScO}_5$  signal is supported by DFT first-principles calculations. The formation of  $\text{ScO}_5$  sites is concomitant with the decrease of water  $^1\text{H}$  NMR signal. Thus, the  $\text{ScO}_5$  sites are produced from  $\text{ScO}_6$  one by the removal of an aqua ligand. The formation of  $\text{ScO}_5$  sites in activated MIL-100(Sc) explains the Lewis acidity of this material.  $^1\text{H}$  NMR also shows the evacuation of the physisorbed molecules from the pores, whereas  $^{45}\text{Sc}$  NMR indicates a change in the local environment of  $\text{ScO}_6$  sites in activated MOFs. Moreover,  $^{13}\text{C}\{-^{45}\text{Sc}\}$  proximities have been probed for the first time using NMR. Even if  $^{13}\text{C}$  and  $^{45}\text{Sc}$  isotopes exhibit close Larmor frequencies the combination of a frequency splitter and an adapted NMR pulse sequence has permitted the estimate of  $^{13}\text{C}\{-^{45}\text{Sc}\}$  distances in MIL-100(Sc). This technique has enabled to detect a shrinkage of the structure when the temperature increases.

## Experimental Section

### Synthesis of materials

**$\text{Sc}_3\text{BTB}_2$ :** It was synthesized, based on an upscale version of the procedure reported in the literature<sup>[16]</sup> using  $\text{ScCl}_3 \cdot x\text{H}_2\text{O}$  (0.27 g, 1.35 mmol) and  $\text{H}_3\text{BTB}$  (0.20 g, 0.45 mmol) dispersed in a mixture of *N,N*-dimethylformamide (DMF, 6 mL), tetrahydrofuran (THF, 8 mL),  $\text{CH}_2\text{Cl}_2$  (6 mL),  $\text{H}_2\text{O}$  (6 mL) and  $\text{HNO}_3$  (69.5%, 6 drops). The reaction was carried out in a 125 mL Teflon-liner within a Parr-type autoclave heated at 120°C for 48 h and then cooled down to room temperature over a period of 12 h.

**MIL-100(Sc):** This compound was synthesized according to the procedure reported in the literature and  $\text{Sc}(\text{NO}_3)_3 \cdot 3\text{H}_2\text{O}$  was used as the scandium source.<sup>[6]</sup>

### Thermodiffraction

Thermodiffractions of Sc<sub>3</sub>BTB<sub>2</sub> and MIL-100(Sc) were performed under 5 L.h<sup>-1</sup> air flow in an Anton Paar HTK1200N of a D8 Advance Bruker diffractometer ( $\theta$ - $\theta$  mode, CuK $\alpha_{1/2}$  radiation) equipped with a Vantec1 linear position sensitive detector (PSD). Each powder pattern was recorded in the range 6-60° for 2 $\theta$  (at intervals of 20°C between RT and 800°C) with a 1s/step scan, corresponding to an approximate duration of 27 min. The heating rate between two patterns was 5°C.min<sup>-1</sup>.

The PXRD analysis for the Sc<sub>3</sub>BTB<sub>2</sub> rehydrated sample was carried out on a Bruker D8 Advance diffractometer (CuK $\alpha$  radiation) equipped with a Lynx Eye® fast detector. Each pattern was recorded in the 2 $\theta$  range 5-50° with a 0.3 s/step scan.

### Sample preparation for NMR measurements

**Sc<sub>3</sub>BTB<sub>2</sub>.** As described in the literature,<sup>[16]</sup> as-synthesized product was first soaked in acetone during 96 h, and then degassed under vacuum (10<sup>-6</sup> bar) at the desired temperature (170, 275 or 325°C) overnight. The resulting product was then cooled down to room temperature and transferred in an argon glovebox to be packed in a 3.2 mm zirconia rotor, which was closed with a Vespel cap.

**MIL-100(Sc).** As-synthesized samples were packed in a 3.2 mm zirconia rotor without a cap and heated in an oven at the desired temperature (100, 150, 220 or 300°C) for one night. At the end of the night, the rotor was closed with a Vespel cap.

### NMR experiments

The employed NMR pulse sequences are depicted in Figs. S1-S3 of the Electronic Supporting Information. The <sup>1</sup>H and <sup>13</sup>C chemical shifts were referenced to tetramethylsilane (TMS), whereas the <sup>45</sup>Sc chemical shifts were referenced to 1M Sc(NO<sub>3</sub>)<sub>3</sub>.3H<sub>2</sub>O aqueous solution.

For both MIL-100(Sc) and Sc<sub>3</sub>BTB<sub>2</sub> samples, <sup>1</sup>H, <sup>45</sup>Sc and <sup>45</sup>Sc-<sup>1</sup>H NMR experiments were carried out using a Bruker Avance III 18.8 T (800 MHz for proton) spectrometer equipped with a 3.2 mm double resonance probe spinning at a Magic-Angle Spinning (MAS) frequency of  $\nu_R = 20$  kHz. In the <sup>1</sup>H experiments, a DEPTH sequence was used to remove the background signal,<sup>[31]</sup> and the RF-amplitude was 73 and 71 kHz for MIL-100(Sc) and Sc<sub>3</sub>BTB<sub>2</sub> respectively. The <sup>45</sup>Sc NMR spectra were acquired using direct excitation under MAS (DEMAs) using a <sup>45</sup>Sc pulse lasting 0.93  $\mu$ s and an RF amplitude of 67 kHz for MIL-100(Sc) and 1  $\mu$ s and an RF amplitude of 62.5 kHz for Sc<sub>3</sub>BTB<sub>2</sub>. The <sup>1</sup>H DEMAs spectra result from averaging 16 transients with a recovery delay  $\tau_{RD} = 5$  s, i.e. an experimental time of 80 s. The <sup>45</sup>Sc DEMAs spectra result from averaging 1024 transients with a recovery delay  $\tau_{RD} = 0.5$  s, i.e. an experimental time of 8 min 32 s.

For the dipolar-mediated Heteronuclear Multiple-Quantum Correlation (D-HMQC) 2D experiments with <sup>45</sup>Sc detection and <sup>1</sup>H indirect detection (<sup>45</sup>Sc-<sup>1</sup>H}), the heteronuclear coherence transfer is mediated by <sup>1</sup>H-<sup>45</sup>Sc dipolar interactions, which are reintroduced by the SR4<sub>2</sub> symmetry-based recoupling sequence.<sup>[32]</sup> This recoupling scheme suppresses the homonuclear <sup>1</sup>H-<sup>1</sup>H dipolar interactions in the first-order average Hamiltonian.<sup>[33]</sup> <sup>1</sup>H RF amplitudes for the 90° pulses and the SR4<sub>2</sub> recoupling were equal to  $\nu_{rf} = 71$  and 40 kHz (twice  $\nu_R$ ), respectively. The RF amplitude of the <sup>45</sup>Sc pulses selective of the Central Transition (CT) was equal to 18 kHz. Each of the two dipolar recoupling periods,  $\tau_{rec}/2$ , was equal to 600  $\mu$ s = 12T<sub>R</sub> (where T<sub>R</sub> corresponds to a rotor period). No <sup>1</sup>H dipolar decoupling was applied during the acquisition. Spectra were recorded with an accumulation of 600 transients and a recovery delay of  $\tau_{RD} = 1$  s, leading to an experimental time of 8 hours.

<sup>45</sup>Sc triple-quantum (3Q-MAS) 2D experiments were acquired using a z-filtered pulse sequence.<sup>[34]</sup> Excitation and reconversion pulses lasted 3.5 and 1.0  $\mu$ s, respectively, with  $\nu_{rf} = 62.5$  kHz for Sc<sub>3</sub>BTB<sub>2</sub> and 3.6 and 1.2  $\mu$ s with  $\nu_{rf} = 52$  kHz for MIL-100(Sc). The CT selective  $\pi/2$  last pulse

employed  $\nu_{rf} = 7.6$  and 9 kHz for MIL-100(Sc) and Sc<sub>3</sub>BTB<sub>2</sub>, respectively. The recovery delay, the number of transients and the experimental time were (0.5 s, 960, 6h30) for Sc<sub>3</sub>BTB<sub>2</sub> and (2 s, 504, 12 h) for MIL-100(Sc). The <sup>45</sup>Sc quintuple-quantum MAS (5Q-MAS) spectra of MIL-100(Sc) were also acquired (not shown) but they exhibit similar resolution as the 3Q-MAS ones and lower signal-to-noise ratio (S/N).

The <sup>1</sup>H → <sup>13</sup>C cross-polarization (CPMAS) 1D experiments and the Resonance-Echo Saturation-Pulse DOuble-Resonance (RESPDOR) one with <sup>13</sup>C detection and <sup>45</sup>Sc as dephaser nuclei (<sup>13</sup>C-<sup>45</sup>Sc) were performed on a 9.4 T Bruker spectrometer (400 MHz for proton) equipped with an AVANCE-II console. Spectra were recorded with a 3.2 mm three-channels HXY probe used in double-resonance mode and the rotor was spun at  $\nu_R = 12.5$  kHz. For the <sup>1</sup>H → <sup>13</sup>C CPMAS 1D experiments of MIL-100(Sc), the recovery delay was  $\tau_{RD} = 2$  s, the contact time was  $\tau_{CP} = 3$  ms, the <sup>13</sup>C RF field was 94 kHz, and the <sup>1</sup>H RF field amplitude was linearly ramped from 50 to 100 kHz. SPINAL-64 <sup>1</sup>H decoupling with 80 kHz rf was applied during the acquisition of <sup>13</sup>C spectra.<sup>[35]</sup> The number of scans was NS = 512, which lead to 17 minutes experimental time.

<sup>13</sup>C-<sup>45</sup>Sc RESPDOR experiments employ Simultaneous Frequency and Amplitude Modulation (SFAM<sub>1</sub>) scheme<sup>[36]</sup> as heteronuclear dipolar recoupling and are denoted SFAM-RESPDOR hereafter. The SFAM<sub>1</sub> heteronuclear recoupling has been chosen because it is robust and efficient when the irradiated spins are not subject to large homo-nuclear dipolar couplings, as it is the case here for the <sup>13</sup>C nuclei in this isotopically unmodified MOFs. In RESPDOR experiments, the RF field amplitude of <sup>45</sup>Sc saturation pulse was 50 kHz, and the sum of the two dipolar SFAM<sub>1</sub> recoupling periods,  $\tau_{rec}$ , was varied from 0 to 4 ms. Continuous wave <sup>1</sup>H decoupling with an RF field amplitude of 80 kHz was applied during SFAM<sub>1</sub> recoupling periods. SPINAL-64 <sup>1</sup>H decoupling with  $\nu_{rf} = 80$  kHz was also applied during acquisition. The recovery delay of this experiment was  $\tau_{RD} = 2$  s. The number of scans was NS = 2048 and the experiments lasted for 23 hours.

### First-principles calculations

Calculations were performed with the CASTEP DFT code (version 8)<sup>[37]</sup> using the GIPAW (gauge including projected augmented wave) algorithm.<sup>[37, 38]</sup> Perdew-Burke-Ernzerhof generalized gradient approximation<sup>[39]</sup> was used and the valence electrons were described by ultra-soft pseudopotentials.<sup>[40]</sup> The integrals over the first Brillouin zone were performed using a Monkhorst-Pack grid<sup>[41]</sup> and k point spacing was 0.04 2 $\pi$  Å<sup>-1</sup>. The cut-off energy used was 60 Ry. Scalar relativistic effects were included at the zero-order relativistic approximation (ZORA) level.<sup>[42]</sup> A semi-empirical dispersion correction (SEDC) scheme was used.<sup>[43]</sup> DFT calculations were first performed on the already published structure of MIL-88(Sc)<sub>2</sub><sup>[30]</sup> which contains six ScO<sub>6</sub> sites. Then, the crystallographic data of MIL-88(Sc) containing ScO<sub>5</sub> sites were derived by removing one H<sub>2</sub>O molecule from the MIL-88(Sc) unit cell. This modified unit cell contains five ScO<sub>6</sub> sites and one ScO<sub>5</sub> site.

Geometry optimizations of the structures were performed using a variable unit cell with an energy tolerance of 0.0001 eV. The <sup>45</sup>Sc isotropic chemical shifts were referenced by converting the absolute magnetic shielding  $\sigma_{iso,i}$  into the chemical shift  $\delta_{iso,i} = \sigma_{ref,i} - \sigma_{iso,i}$  so that  $\delta_{iso}(\text{<sup>45</sup>Sc}) = -48.2$  ppm for ScPO<sub>4</sub>.

### Acknowledgements

Chevreur Institute (FR 2638), Ministère de l'Enseignement Supérieur et de la Recherche, Région Hauts-de-France and FEDER are acknowledged for supporting and funding partially this work. Authors are also grateful for funding supported by

contract ANR-14-CE07-0009-01. Laurence Burylo and Frédéric Capet are also acknowledged for the help with the X-Ray Diffraction.

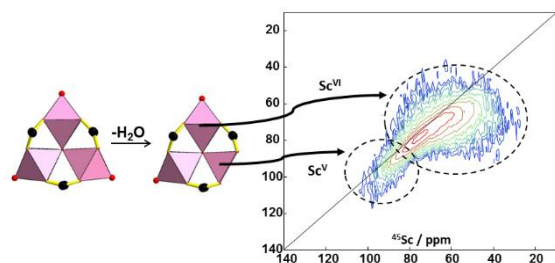
**Keywords:** MOF • MIL-100(Sc) • ScO<sub>5</sub> • DFT • <sup>13</sup>C-<sup>45</sup>Sc

- [1] H. C. Zhou, J. R. Long, O. M. Yaghi, *Chem. Rev.* **2012**, *112*, 673-1268; J. R. Long, O. M. Yaghi, *Chem. Soc. Rev.* **2009**, *38*, 1207-1508.
- [2] C. Serre, F. Millange, S. Surble, G. Férey, *Angew. Chem.-Int. Ed.* **2004**, *43*, 6286-6289.
- [3] P. Horcajada, S. Surble, C. Serre, D.-Y. Hong, Y.-K. Seo, J.-S. Chang, J.-M. Greneche, I. Margiolaki, G. Férey, *Chem. Commun.* **2007**, 2820-2822.
- [4] C. Volkringer, D. Popov, T. Loiseau, G. Férey, M. Burghammer, C. Riekell, M. Haouas, F. Taulelle, *Chem. Mater.* **2009**, *21*, 5695-5697.
- [5] A. Lieb, H. Leclerc, T. Devic, C. Serre, I. Margiolaki, F. Mahjoubi, J. S. Lee, A. Vimont, M. Daturi, J. S. Chang, *Microporous Mesoporous Mater.* **2012**, *157*, 18-23.
- [6] J. P. S. Mowat, S. R. Miller, A. M. Z. Slawin, V. R. Seymour, S. E. Ashbrook, P. A. Wright, *Microporous Mesoporous Mater.* **2011**, *142*, 322-333.
- [7] Y. T. Li, K. H. Cui, J. Li, J. Q. Zhu, X. Wang, Y. Q. Tian, *Chin. J. Inorg. Chem.* **2011**, *27*, 951-956.
- [8] F. Zhang, X. Q. Zou, W. Feng, X. J. Zhao, X. F. Jing, F. X. Sun, H. Ren, G. S. Zhu, *J. Mater. Chem.* **2012**, *22*, 25019-25026.
- [9] A. Vimont, J. M. Goupil, J. C. Lavalley, M. Daturi, S. Surble, C. Serre, F. Millange, G. Férey, N. Audebrand, *J. Am. Chem. Soc.* **2006**, *128*, 3218-3227.
- [10] M. Haouas, C. Volkringer, T. Loiseau, G. Férey, F. Taulelle, *J. Phys. Chem. C* **2011**, *115*, 17934-17944.
- [11] A. Vimont, H. Leclerc, F. Mauge, M. Daturi, J. C. Lavalley, S. Surble, C. Serre, G. Férey, *J. Phys. Chem. C* **2007**, *111*, 383-388.
- [12] C. Volkringer, D. Popov, T. Loiseau, N. Guillou, G. Férey, M. Haouas, F. Taulelle, C. Mellot-Draznieks, M. Burghammer, C. Riekell, *Nature Mater.* **2007**, *6*, 760-764.
- [13] C. Volkringer, H. Leclerc, J. C. Lavalley, T. Loiseau, G. Férey, M. Daturi, A. Vimont, *J. Phys. Chem. C* **2012**, *116*, 5710-5719.
- [14] J. Perles, M. Iglesias, C. Ruiz-Valero, N. Snejko, *Chem. Commun.* **2003**, 346-347; L. Mitchell, P. Williamson, B. Ehrlichova, A. E. Anderson, V. R. Seymour, S. E. Ashbrook, N. Acerbi, L. M. Daniels, R. I. Walton, M. L. Clarke, P. A. Wright, *Chem. Eur. J.* **2014**, *20*, 17185-17197; Y. Cao, Z. Q. Zhu, J. N. Xu, L. Wang, J. Y. Sun, X. B. Chen, Y. Fan, *Dalton Trans.* **2015**, *44*, 1942-1947.
- [15] L. Mitchell, B. Gonzalez-Santiago, J. P. S. Mowat, M. E. Gunn, P. Williamson, N. Acerbi, M. L. Clarke, P. A. Wright, *Catal. Sci. Technol.* **2013**, *3*, 606-617.
- [16] I. A. Ibarra, X. Lin, S. Yang, A. J. Blake, G. S. Walker, S. A. Barnett, D. R. Allan, N. R. Champness, P. Hubberstey, M. Schroeder, *Chem. Eur. J.* **2010**, *16*, 13671-13679.
- [17] N. Kim, C. H. Hsieh, J. F. Stebbins, *Chem. Mater.* **2006**, *18*, 3855-3859.
- [18] N. Kim, J. F. Stebbins, *Chem. Mater.* **2009**, *21*, 309-315.
- [19] A. J. Rossini, R. W. Schurko, *J. Am. Chem. Soc.* **2006**, *128*, 10391-10402.
- [20] M. D. Alba, P. Chain, P. Florian, D. Massiot, *J. Phys. Chem. C* **2010**, *114*, 12125-12132.
- [21] C. V. Chandran, J. Cuny, R. Gautier, L. Le Polles, C. J. Pickard, T. Brauniger, *J. Magn. Reson.* **2010**, *203*, 226-235.
- [22] T. Brauniger, A. J. Hofmann, I. L. Moudrakovski, C. Hoch, W. Schnick, *Solid State Sci.* **2016**, *51*, 1-7.
- [23] J. Haase, N. J. Curro, C. P. Slichter, *J. Magn. Reson.* **1998**, *135*, 273-279.
- [24] F. Pourpoint, J. Trébosc, R. M. Gauvin, Q. Wang, O. Lafon, F. Deng, J. P. Amoureux, *ChemPhysChem* **2012**, *13*, 3605-3615.
- [25] F. Pourpoint, Y. Morin, R. M. Gauvin, J. Trébosc, F. Capet, O. Lafon, J. P. Amoureux, *J. Phys. Chem. C* **2013**, *117*, 18091-18099; F. Pourpoint, A. S. Lilly Thankamony, C. Volkringer, T. Loiseau, J. Trébosc, F. Aussenac, D. Carnevale, G. Bodenhausen, H. Vezin, O. Lafon, J. P. Amoureux, *Chem. Commun.* **2014**, *50*, 933-935.
- [26] F. Pourpoint, J. Yehl, M. Li, R. Gupta, J. Trébosc, O. Lafon, J.-P. Amoureux, T. Polenova, *ChemPhysChem* **2015**, *16*, 1619-1626.
- [27] C. Volkringer, T. Loiseau, M. Haouas, F. Taulelle, D. Popov, M. Burghammer, C. Riekell, C. Zlotea, F. Cuevas, M. Latroche, D. Phanon, C. Knofel, P. L. Llewellyn, G. Férey, *Chem. Mater.* **2009**, *21*, 5783-5791.
- [28] D. I. Kolokolov, H. Jovic, A. G. Stepanov, V. Guillerm, T. Devic, C. Serre, G. Férey, *Angew. Chem.-Int. Ed.* **2010**, *49*, 4791-4794.
- [29] I. Oikawa, H. Takamura, *Chem. Mater.* **2015**, *27*, 6660-6667.
- [30] P. D. C. Dietzel, R. Blom, H. Fjellvag, *Dalton Trans.* **2006**, 2055-2057.
- [31] D. G. Cory, W. M. Ritchey, *J. Magn. Reson.* **1988**, *80*, 128-132.
- [32] A. Brinkmann, A. P. M. Kentgens, *J. Am. Chem. Soc.* **2006**, *128*, 14758-14759.
- [33] O. Lafon, Q. Wang, B. W. Hu, F. Vasconcelos, J. Trébosc, S. Cristol, F. Deng, J. P. Amoureux, *J. Phys. Chem. A* **2009**, *113*, 12864-12878.
- [34] J. P. Amoureux, C. Fernandez, S. Steuernagel, *J. Magn. Reson.* **1996**, *123*, 116-118.
- [35] B. M. Fung, A. K. Khitrin, K. Ermolaev, *J. Magn. Reson.* **2000**, *142*, 97-101.
- [36] R. Q. Fu, S. A. Smith, G. Bodenhausen, *Chem. Phys. Lett.* **1997**, *272*, 361-369.
- [37] C. J. Pickard, F. Mauri, *Phys. Rev. B* **2001**, *63*, 245101(245101-245113).
- [38] C. Bonhomme, C. Gervais, F. Babonneau, C. Coelho, F. Pourpoint, T. Azais, S. E. Ashbrook, J. M. Griffin, J. R. Yates, F. Mauri, C. J. Pickard, *Chem. Rev.* **2012**, *112*, 5733-5779; T. Charpentier, *Solid State Nucl. Magn. Reson.* **2011**, *40*, 1-20; S. E. Ashbrook, D. McKay, *Chem. Commun.* **2016**, *52*, 7186-7204.
- [39] J. P. Perdew, K. Burke, M. Ernzerhof, *Phys. Rev. Lett.* **1996**, *77*, 3865-3868.
- [40] D. Vanderbilt, *Phys. Rev. B* **1990**, *41*, 7892-7895.
- [41] H. J. Monkhorst, J. D. Pack, *Phys. Rev. B* **1976**, *13*, 5188-5192.
- [42] T. F. G. Green, J. R. Yates, *J. Chem. Phys.* **2014**, *140*.
- [43] D. V. Dudenko, J. R. Yates, K. D. M. Harris, S. P. Brown, *CrystEngComm* **2013**, *15*, 8797-8807.



## Entry for the Table of Contents

## FULL PAPER



R. Giovine, C. Volkringer, S. E. Ashbrook,  
J. Trébosc, D. McKay, T. Loiseau, J.-P.  
Amoureux, O. Lafon, F. Pourpoint\*

Page No. – Page No.

Solid-state NMR proves the presence  
of penta-coordinated Sc site in MIL-  
100(Sc)